

Eclipse Timing Modeling of Three Post-Common Envelope Binaries: Hybrid Solutions

Xinyu Mai,^{1*} Robert L. Mutel^{1†}

¹*Department of Physics and Astronomy, University of Iowa, Iowa City, IA 52242, USA*

Accepted XXX. Received YYY; in original form ZZZ

ABSTRACT

We report 88 new observations of three post common envelope binaries at primary eclipse spanning between December 2018 to February 2021. We combine recent primary eclipse timing observations with previously published values to search for substellar circumbinary components consistent with timing variations from a linear ephemeris. We used a least-squares minimization fitting algorithm weighted by a Hill orbit stability function, followed by Bayesian inference, to determine best-fit orbital parameters and associated uncertainties. For HS2231+2441, we find that the timing data are consistent with a constant period and that there is no evidence to suggest orbiting components. For HS0705+6700, we find both two and three-component solutions that are stable for at least 10 Myr but have very different parameters. For HW Vir, we find multi-component solutions that fit the timing data but they are unstable on short timescale, and therefore highly improbable. Conversely, both the least-squares and Bayesian solutions provide a poor fit. In both systems, the best-fit stable solutions significantly deviate from the ensemble timing data.

For both HS0705+6700 and HW Vir, substellar component solutions that fit all observed eclipse timing data are dynamically unstable, whereas best-fit solutions with stable orbits provide poor O-C fits. We speculate that the observed timing variations for these systems, and very possibly other sdB binaries, may result from a combination of substellar component perturbations and an Applegate-Lanza mechanism.

Key words: binaries: close - binaries: eclipsing - stars: individual: HW Vir, HS0705+6700, HS2231+2441 - planetary systems

1 INTRODUCTION

Since the discovery of the first extra-solar planets nearly 30 years ago (Wolszczan & Frail 1992; Mayor & Queloz 1995), more than 4,000 exoplanetary systems have been discovered, mostly orbiting late-type single stars (Martin 2018). However, more than 100 planet-hosting multiple-star systems have also been found (Schwarz et al. 2016), perhaps not surprisingly since a substantial fraction of all stars are in multiple systems (Tokovinin 2014).

An intriguing subset of these planet-hosting binaries are evolved short-period binaries. In these systems, the more massive star has evolved off the main sequence and lost nearly all of its hydrogen envelope during the red-giant phase, filling its Roche lobe and generating unstable mass transfer to the secondary star (Icko & Livio 1993). Since the timescale for mass transfer is much shorter than the thermal timescale of the secondary, a common envelope forms surrounding both components. The orbiting stars experience drag forces, transferring angular momentum to the envelope and causing it to expand and eventually be expelled (Webbink 1984; Zorotovic et al. 2010; Ivanova et al. 2013). This leaves a hot B-star or white dwarf with a low mass main-sequence companion separated by a few solar radii, and consequent orbital period of a few hours (Nebo

Gómez-Morán et al. 2011; Heber 2009). These systems are referred to as post common-envelope binaries (PCEB).

Eclipsing PCEBs provide a sensitive probe of potential substellar companions, since the eclipses are frequent and deep, and can be timed with high accuracy. This allows one to infer the presence of orbiting substellar companions by modeling the observed eclipse timing variations (ETV's) caused by the reflex motion of the binary's barycenter due to the substellar companion[s].

To date, more than a dozen eclipsing PCEBs have been observed to exhibit large, occasionally erratic changes in their orbital period (Heber 2016). If these timing variations are caused by circumbinary substellar components, they must have either survived the common envelope phase, or have been formed from the common envelope debris, and therefore be much younger than the parent stars. This 'second generation' scenario is considered more likely for PCEBs by some authors (Zorotovic & Schreiber 2013; Schleicher & Dreizler 2014; Schleicher et al. 2015), but this hypothesis is still controversial. For example, Bear & Soker (2014) argue that too large a fraction of the common envelope mass would have to form into substellar companions for this to be viable.

Detailed modeling of eclipse timing variations (ETV) has resulted in the claimed detection of multiple circumbinary companions, either brown dwarfs or massive planets, in at least ten PCEBs (Marsh 2018). However, these claims are not universally accepted: Several of the proposed planetary orbits have been shown to be dynamically unstable over timescales much shorter than would be consistent with

* E-mail: xinyu-mai@ku.edu

† E-mail: robert-mutel@uiowa.edu

even the ‘second generation’ planetary formation hypothesis (Horner et al. 2012; Horner et al. 2014; Wittenmyer et al. 2013).

Alternative explanations for observed eclipse timing variation in binary stars have been considered, including apsidal precession (Shakura 1985; Parsons et al. 2013) and changes in the mass quadrupole moment of the secondary star caused by magnetic activity, a.k.a. the Applegate mechanism (Applegate & Patterson 1987; Applegate 1992; Lanza et al. 1998; Lanza 2006; Beuermann et al. 2012b; Lanza 2020). Apsidal precession, which results from a small non-zero eccentricity of the binary orbit, appears unlikely, since it would require eccentricities of order $e \sim 0.01$ to explain observed PCEB eclipse timing variations (~ 100 sec). These could be ruled out by observing primary to secondary eclipse timing asymmetries, which would be of the same order as the observed ETV variations, and would have a periodic time shift of the secondary eclipse with respect to phase 0.5. In one case (HW Vir), Baran et al. (2018) reported no significant deviation from phase 0.5 for secondary eclipse times observed over 70 days. Furthermore, ETV’s from PCEB binaries are typically aperiodic, whereas apsidal precession would result in smooth timing variations over an orbital period.

The Applegate mechanism has been considered to explain PCEB ETV’s by several authors (e.g. Qian et al. (2008); Lee et al. (2009); Wittenmyer et al. (2012); Nasiroglu et al. (2017)). However, detailed stellar models of the angular momentum exchange between a finite shell and the core of the secondary star show that the required energy to produce the quadrupole moment variations is too high in most PCEB systems, including all three of those described here (Völschow, M. et al. 2016; Navarrete, F. H. et al. 2018; Navarrete et al. 2019). However, recently (Lanza 2020) has proposed a new model based on the angular momentum exchange between the spin of the magnetically active secondary and the binary orbital motion. This mechanism may overcome the energy limitations of the original Applegate mechanism, and could contribute to the observed eclipse timing variations.

In this paper, we report new primary eclipse timing observations of three PCEB systems, combining them with previously published observations to solve for possible substellar companions that can account for the observed timing variations. We also analyze the orbital stability of the proposed systems using numerical simulation of orbital dynamics and testing for chaotic behavior over long timescales.

This procedure could be considered fraught and even unproductive, since it is typically degenerate (fitted model parameters are typically highly correlated) and almost all previously proposed planetary models have failed to correctly predict subsequent ETV observations. Indeed, as Marsh (2018) recently pointed out, there is no *independent* evidence for any substellar companion deduced from ETV variations in PCEBs. Nevertheless, the ETV variations are clearly real and all alternate explanations have so far failed with compelling physical arguments. Hence, both Occam’s razor and the scientific method encourage us to assume the most plausible hypothesis, find physical models that are in agreement with the observations, and most importantly, provide predictions that future observations can test.

1.1 HW Virginis

HW Vir ($V = 10.7$, $P = 2.8$ hr) is the prototype of the eponymous HW Vir class of eclipsing subdwarf B stars with low-mass dwarf companions. Variations in the orbital period were first discovered by Kilkenny et al. (1994), who reported a period decrease over nine years. Subsequent ETV studies of HW Vir have been carried out by several authors (Çakirli & Devlen 1999; Kiss et al. 2000; Kilkenny et al. 2000, 2003; İbanoğlu et al. 2004; Lee et al. 2009; Qian et al.

2010; Beuermann et al. 2012b; Skelton 2012; Lohr et al. 2014; Baran et al. 2018; Esmer et al. 2021; Brown-Sevilla et al. 2021). These papers invoked one or more substellar companions as the primary cause of the observed ETVs. However, as new data became available, these models inevitably needed to be modified.

After ruling out mass transfer, magnetic braking, and apsidal motion, Çakirli & Devlen (1999) concluded that a third body with mass $22 M_{\text{Jup}}$ and an orbital period of 19 yr is the most probable cause. İbanoğlu et al. (2004) also proposed a brown dwarf companion, but with a mass twice that of Çakirli et al., and half their period. Lee et al. (2009) proposed two companions with periods 15.8 and 9.1 yrs and masses of $19.2 M_{\text{Jup}}$ and $8.5 M_{\text{Jup}}$ respectively. Beuermann et al. (2012a) added more ETV data, and showed that they deviated significantly from the solution proposed by Lee et al. (2009). They also showed that the solution proposed by Lee et al. is dynamically unstable. They proposed a new solution consisting of two brown dwarfs ($14 M_{\text{Jup}} + 65 M_{\text{Jup}}$) that was stable over more than 10 Myr. However, Baran et al. (2018) showed that the solution of Beuermann et al. does not fit more recent O-C data.

Horner et al. (2012) independently made a stability analysis of the Lee et al. solution, and also found it highly unstable. Indeed, they searched a significant volume of substellar component parameter space, and could not find any stable solutions, concluding "If the [HW Vir] system does host exoplanets, they must move on orbits differing greatly from those previously proposed". This failure to find a stable solution is reinforced by the recent studies of Esmer et al. (2021) and Brown-Sevilla et al. (2021) using all previously published O-C observations along with new times of minima up to 2019.4. They tried a number of multi-planet models but also failed to find a stable solution.

1.2 HS0705+6700

Drechsel et al. (2001) first confirmed HS0705+6700 (V470 Cam, $V = 14.7$, $P = 2.3$ hr) as a post common envelope sdB binary. They fit their eclipsing timing observations with a linear ephemeris. Qian et al. (2009) reported a cyclic change in orbital period and proposed a substellar companion with orbital period of 7.15 years and mass of $40 M_{\text{Jup}}$ is responsible for the observed ETV. Beuermann et al. (2012b) observed an additional 28 epochs, with a similar solution: A single brown dwarf with mass $31 M_{\text{Jup}}$ and orbital period of 8.4 years.

In 2013, Qian et al. (2013) fit a single brown dwarf model with a period 8.87 years and mass $32 M_{\text{Jup}}$, along with a positive quadratic term $dP/dt = +9.8 \times 10^{-9}$ days/year. They ruled out mass transfer and angular momentum loss due to gravitational radiation and magnetic braking as explanations of this period increase. Pulley et al. (2015) showed that the more recent O-C timing data began to diverge from the Qian model. Later in 2018, they confirmed this departure by adding 65 more times of minima (Pulley et al. 2018).

Bogensberger et al. (2017) proposed a new one planet model with a longer orbital 11.8 year period, eccentricity 0.38, and no quadratic term. Recently, Sale et al. (2020) added 20 additional ETV observations though mid-2018. They found a two component solution that fit all published O-C observations, but unfortunately it was highly unstable over a short timescale (1,000 yr) and hence not physically plausible.

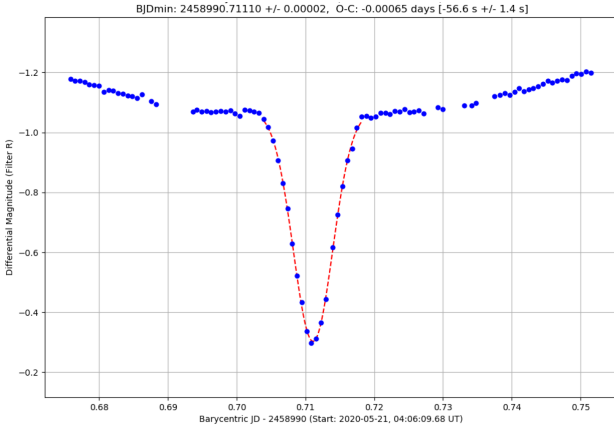


Figure 1. Sample HW Vir light curve taken at the Iowa Robotic Observatory on 21 May 2020 from 04:06 — 06:01 BJD, with fitted Gaussian profile to determine time of minima [red dashed line].

1.3 HS2231+2441

HS2231+2441 ($V = 14.2$, $P = 2.7$ hr) is an eclipsing white dwarf + brown dwarf binary (Almeida et al. 2017) first reported by Østensen et al. (2007). They fit two years of primary eclipse timing observations with a linear (constant period) ephemeris. Qian et al. (2010), using more extensive timing data, reported that the orbital period shows both a cyclic change and a period derivative. They proposed a $14 M_{\text{Jup}}$ component to explain the cyclic variation and magnetic braking to explain the period decrease. However, as more timing observations became available, Lohr et al. (2014) found that a linear function might provide a better fit to the O-C curve. Almeida et al. (2017) reported eight more eclipse times and updated the linear ephemeris. Most recently, Pulley et al. (2018) extended the timing database with 26 more timing minima. They compared the quadratic ephemeris by Qian et al. (2010) and linear ephemeris proposed by Lohr et al. (2014) concluded there is no statistically significant difference between the two.

2 OBSERVATIONS

Our study is an independent analysis of previously published eclipse times and new timing data obtained with the 0.5m telescope at the Iowa Robotic observatory¹, located at Winer Observatory² in south-eastern Arizona. We used a SBIG 6303e CCD camera (2048x3072 x 12 micron pixels) with an field of view 28x18 arcmin. We report 88 new times of minimum for three PCEB systems at primary eclipse between December 2018 and February 2021 (Table 1). A luminance filter was used for HS2231+2441 and HS0705+6700, and an exposure time of 40 sec was adopted. A Sloan r' filter with an exposure time of 15 sec was used for the brighter object HW Vir.

After the normal CCD image calibration including dark frame subtraction and flat fielding, we created light curves using airmass-corrected differential photometry. Both HS 2231+2441 and HS0705+6700 are typical of HW Vir-like eclipsing systems, their light curves show a strong reflection effect with a very deep primary and a shallow secondary minimum. We fit a Gaussian profile

to the primary eclipse light curve using a nonlinear least-squares (Levenberg-Marquardt) algorithm and determine the observed mid-eclipse times. A sample light curve for HW Vir with associated Gaussian profile fit is shown in Fig. 1. We evaluated the uncertainty in time of eclipse minimum by a Monte Carlo method consisting of a series synthetic eclipse light curves with randomly-chosen times of minima and different exposure times. This procedure is described in detail in Appendix 1. Table 2 lists the eclipse timing observations and uncertainties for all three PCEBs.

3 DATA ANALYSIS

3.1 Data selection

Our eclipse timing dataset comprised 88 new time of primary eclipse minima (Table 2) together with previously published times from the literature. Before use, we made a few modifications.

(i) For HW Vir and HS2231+2441, we excluded a portion of archival SuperWASP times of minima that were rejected by Lohr et al. (2014)’s outlier methodology and by the size of their uncertainties. In particular, we did not include Lohr et al. (2014)’s listed extra times of minima due to their precision, and discarded timing data for which uncertainties are between 8 sec ~40 sec. We also took out the individual superWASP times of minima for HS2231+2441 have large ($\sigma > 20\sigma$) uncertainties.

(ii) We also removed O-C eclipse timings obtained from the Mercator observation in Baran et al. (2018) since they deviate from the overall O-C trend line by 50 seconds. We also excluded outliers that had O-C values deviating by more than 400 seconds from the overall O-C trend.

3.2 Light Travel Time Model

For a binary system with orbiting substellar components, the predicted primary mid-eclipse time as a function of cycle number E can be written as

$$T(E) = T_0 + P_0 E + \alpha E^2 + \sum_i \tau_i(E) \quad (1)$$

where T_0 is the reference epoch, P_0 is the linear eclipse period, where τ_i are the time-dependent contributions from each perturbing body, and

$$\alpha = \frac{1}{2} \frac{dP}{dt} P_0, \quad (2)$$

is a quadratic term can would result from non-planetary effects, such as apsidal motion, mass exchange, magnetic braking, or gravitational radiation.

The time signature of perturbing bodies on eclipse timing as a function of each body’s orbital properties is given by Irwin (1952, 1959),

$$\tau_i = \frac{K_i}{\sqrt{1 - [e_i \cos(\omega_i)]^2}} \cdot \left[\frac{1 - e_i^2}{1 + e_i \cos(\nu_i)} \sin(\nu_i + \omega_i) + e_i \sin(\omega_i) \right] \quad (3)$$

where K_i is the semi-amplitude of light travel time delay, e_i denotes the orbital eccentricity, ν_i is the true anomaly and ω_i is the argument of pericenter, with index i indicating each perturbing body in the system.

¹ <http://astro.physics.uiowa.edu/iro>

² <https://winer.org/>

Table 1. Observing Summary

Target	V	N_{obs}	t(sec)	Filter	Epochs
HS2231+2441	14.2	26	40	Luminance	2018.9 – 2020.8
HS0705+6700	14.7	39	40	Luminance	2019.1 – 2021.1
HW Vir	10.7	23	15	Sloan r'	2018.9 – 2021.1

Table 2. Mid-Eclipse Times (BJD)

HS2231+2441	HS0705+6700	HW Vir
2458471.69752(10)	2458500.71590(3)	2459143.84436(5)
2458473.57744(9)	2458504.82867(24)	2459144.89662(6)
2458617.89415(8)	2458505.59376(7)	2459145.85304(4)
2458650.84983(9)	2458512.67178(8)	2459146.80949(6)
2458991.90258(10)	2458565.66003(3)	2459147.86162(4)
2458992.89767(7)	2458589.66736(5)	2459149.87025(6)
2458998.86963(8)	2458619.70026(7)	2459151.87879(7)
2459019.88131(6)	2458847.33965(5) *	2459152.83526(7)
2459020.87669(7)	2458985.74066(17)	2459153.79168(6)
2459021.87188(6)	2458987.74896(6)	2459156.85240(5)
2459022.86704(9)	2458994.73099(8)	2459157.80886(8)
2459023.86254(8)	2459122.89784(5)	2459158.86111(5)
2459024.85779(8)	2459126.91491(6)	2459266.65475(11)
2459026.84836(6)	2459127.87140(6)	
2459138.65276(7)	2459128.92344(7)	
2459139.64791(7)	2459129.88002(6)	
2459140.64330(7)	2459131.88864(5)	
2459141.63860(4)	2459132.84512(5)	
2459142.63383(5)	2459133.89723(4)	
2459143.62915(4)	2459134.85363(6)	
2459144.62452(6)	2459136.86217(5)	
2459145.61985(7)	2459138.87083(7)	
2459146.61505(9)	2459139.82732(8)	
2459147.61035(7)	2459140.87940(6)	
2459151.59148(8)	2459141.83589(5)	
2459152.58676(6)	2459142.88799(6)	
		2458472.00981(2)
		2458473.99404(4)
		2458607.75446(2)
		2458612.77339(2)
		2458621.76088(2)
		2458622.69461(3)
		2458641.019582(41)*
		2458657.71049(3)
		2458981.72376(3)
		2458981.84055(4)
		2458990.71110(2)
		2458992.69525(3)
		2458996.78043(2)
		2458997.71417(2)
		2458998.76469(2)
		2459003.66701(2)
		2459004.71749(2)
		2459020.70807(3)
		2459022.69231(4)
		2459024.67650(3)
		2459263.83482(3)
		2459265.81903(3)
		2459269.78746(3)

NOTE - * Times of minima with asterisk are unpublished observations from David Pulley, John Mallet and the Altair Group. *a.* HS0705+6700 - Dec 29th, 2019. *b.* HW Vir - June 6th, 2019.

Table 3. Binary star physical properties

Binary	Type	M_{pri}	M_{sec}	R_{pri}	R_{sec}	L_{sec}	P_{orb} [d]	Refs
HS2231+2441	WD+BD	0.288	0.046	0.165	0.086	0.0009	0.1106	Almeida et al. (2017)
HS0705+6700	sdB+M4-5	0.483	0.134	0.230	0.186	0.0022	0.0956	Drechsel et al. (2001)
HW Virginis	sdB+M4-5	0.485	0.142	0.183	0.175	0.0025	0.1167	Lee et al. (2009)

NOTE - *a.* All masses, radii, and luminosities are solar units. *b.* [Almeida et al. \(2017\)](#) presents two mass solutions for HS2231: We have listed solution 2. *c.* [Baran et al. \(2018\)](#) derived a primary mass $0.26 M_{\odot}$ for HW Vir, but argue that it is probably an underestimate.

3.3 Orbit stability

A physically credible model must not only fit all the current and previously published ETV datasets, but it is also subject to the prior constraint that the substellar components must be stable to orbital instabilities over timescales at least comparable to the lifetime of the

PCEB phase (~ 100 Myr) ([Han et al. 2002](#); [Han et al. 2003](#); [Zorotovic et al. 2011](#)). To characterize this, we used the Hill stability criterion ([Gladman 1993](#); [Chambers et al. 1996](#)) which predicts whether any two components in orbit about a massive central body will avoid mutual close encounters over many orbits.

For circular orbits, stability occurs if the semi-major axis difference between pairs of components exceeds a critical distance Δ given by (Chambers et al. 1996),

$$\Delta \approx 2\sqrt{3} \cdot R_H \quad (4)$$

where R_H is the Hill radius,

$$R_H = \frac{a_1 + a_2}{2} \left[\frac{(m_1 + m_2)}{3M} \right]^{\frac{1}{3}} \quad (5)$$

where m_1, m_2 and a_1, a_2 are the masses and semi-major axes of the components respectively, and M is the mass of the central body.

For non-circular orbits, a more general stability criterion is (Hasegawa & Nakazawa 1990)

$$\Delta^2 = \left[12 + \frac{4}{3} K^2 e^2 \right] R_H^2 \quad (6)$$

where

$$K = \left[\frac{(m_1 + m_2)}{3M} \right]^{\frac{1}{3}}, \quad (7)$$

and e is the larger eccentricity. For low eccentricity orbits and $K \ll 1$, we can expand the second term to obtain

$$\Delta = 2\sqrt{3} R_H \cdot \left(1 + \frac{K^2 e^2}{18} \right). \quad (8)$$

The second term in parentheses is much less than 1 for the components considered here ($K \ll 1$) so the simpler expression equation 4 was used in our calculations.

We can define a dimensionless parameter β that characterizes each planet pair spacing in terms of the normalized mutual Hill radii as (cf. Smullen et al. 2016)

$$\beta = \frac{|a_2 - a_1|}{\Delta} \quad (9)$$

Stable component pairs correspond to $\beta > 1$ while unstable pairs have $\beta < 1$.

For systems with more than two substellar components, instability can occur even if all components lie outside the Hill radius of their nearest companion, although the timescale for close encounters increases as the initial component separations become larger (Chambers et al. 1996). Hence, we used the Hill parameter as an optimization prior but ran numerical orbit simulations to test orbit stability after optimization, as described below.

3.4 Model Fitting Scheme

The model fitting scheme comprised four steps (Fig. 3):

(i) Create an initial model of either two, three, or four sub-stellar components mutually spaced at least one Hill radius apart (i.e., $\beta > 1$ for all pairs),

(ii) Search for the minimum of an objective function proportional to the product of the summed χ^2 of the model vs. O-C time series and an ansatz 'penalty' function that sharply increases when the smallest Hill parameter β becomes less than 1.0 for any component pair,

(iii) Use Bayesian inference to solve for the final fitted parameters using a Markov chain Monte Carlo (MCMC) sampling, a weighted least-squares objective function, and an orbit stability prior ($\beta > 1$),

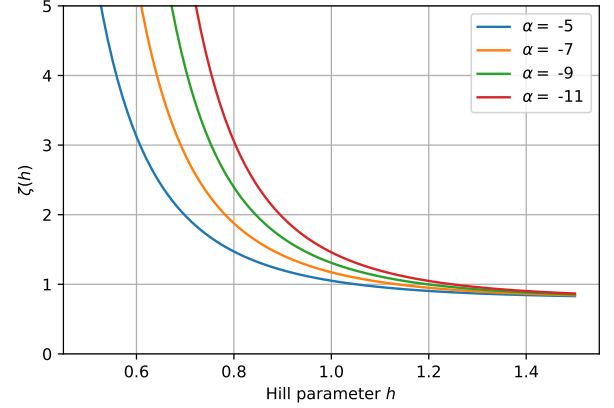


Figure 2. Hill penalty function used in prior function (see text). (Eqn. 11).

(iv) Run orbit stability tests using both the N-body orbital integration package REBOUND (Rein & Liu 2012; Rein & Spiegel 2015) and the chaotic indicator program MEGNO (Cincotta & Simó 2000; Hinse et al. 2010).

We first chose the number of substellar companions to model. Examination of the O-C plot for both HS0705+6700 and HW Virginis indicates that a single companion would prove inadequate since it would result in a strictly periodic O-C curve which is not observed. Likewise, a large number of components, although certainly possible, is not justified by the data, since the model parameters are already highly degenerate for few component models, as we will see. Hence we restrict our model selection to 2, 3, and 4-component models. Each component is characterized by four parameters: mass, semi-major axis, eccentricity, and argument of pericenter. We restricted the model to co-planar orbits for the sake of computational simplicity. We also added a period derivative parameter to account for the possible contribution of non-orbiting components, such as apsidal motion or gravitational radiation.

We started model fitting using a downhill simplex (Nelder-Mead) minimization (Python library LMFIT³ to fit the O-C curve. However, instead of minimizing the sum-squared differences between the O-C data and the model, we incorporate the orbit stability constraint by minimizing the product,

$$\zeta \cdot \chi^2 \quad (10)$$

Where we define an empirical Hill stability function

$$\zeta = 0.8 \tanh(2\beta_{\min} - 0.2)^{-\alpha} \quad (11)$$

where the Hill parameter β_{\min} is the smallest normalized Hill parameter (equation 9) of all component pairs. This stability function asymptotes to unity for $\beta > 1$ but increases sharply for $\beta < 1$ (see Fig.2).

The resulting model was used as a starting point for Bayesian inference modeling. We used the EMCEE (Foreman-Mackey et al. 2013) Python implementation⁴ with 2048 walkers and 1500 iterations. The likelihood function was summed-squared difference between the model and O-C data weighted by the data uncertainties. We

³ <https://lmfit.github.io/lmfit-py>

⁴ <https://github.com/dfm/emcee>

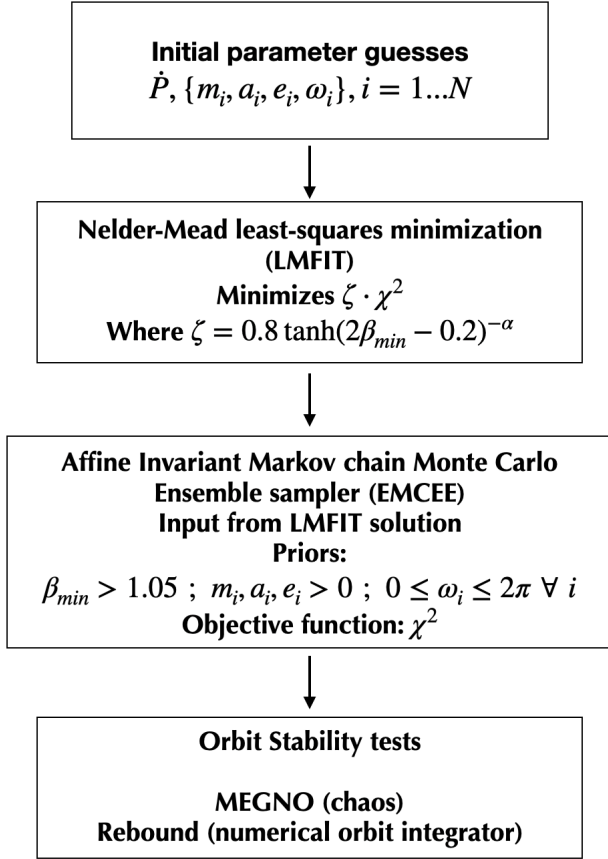


Figure 3. Flow chart of data analysis.

used three priors: (i) stability parameter $\beta > 1.05$, (ii) all masses and semi-major axes positive-definite, and (iii) eccentricities restricted to the range $0 < e < 1$.

Using a model fitting scheme with a Bayesian methodology as the final step has two important advantages over the more commonly-used frequentist least-squares minimization approach. First, the orbit stability constraint (Hill parameter) can be incorporated naturally as a Bayesian prior without the *ad hoc* ansatz function we used in the LMFIT minimization. Second, the Bayesian posterior distribution provides a more comprehensive description of the parameter uncertainties and correlations.

For each model, we tested dynamical stability by numerically integrating the component orbits using WHFAST, a Wisdom-Holman symplectic integrator (Rein & Tamayo 2015). We used a time step of 36.5 days and integrated for 10 Myr for each model. In addition, we tested for chaotic behavior using the MEGNO algorithm (Mean Exponential Growth factor of Nearby Orbits, Cincotta & Simó (2000)) also with a time interval of 10 Myr. Both WHFAST and MEGNO were called from the Python package REBOUND (Rein & Liu 2012) which also provided convenient tools for plotting orbits and time histories of orbital elements.

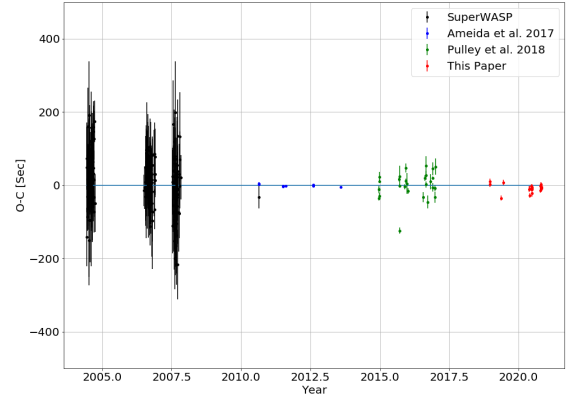


Figure 4. HS2231+2441 O-C times of primary minima computed using the linear ephemeris given in Equation 12. Observations shown as blue data points are times of minima from Almeida et al. (2017), while green points are from Pulley et al. (2018), and red points are new times of minima (Table 2).

4 RESULTS

4.1 HS2231+2441

After adding 26 additional primary eclipse timing observations (listed in Table 2) to previously published observations, we fit the linear ephemeris of Almeida et al. (2017) with a slightly changed orbital period,

$$\text{BJD}_{\min} = 2455428.76185(10) + 0.11058786(10) \cdot E \quad (12)$$

The O-C diagram with all of the available data is shown in Figure 4.

We find that there is no statistically significant period variation for HS2231+2441 spanning 16 years, from 2004 to 2020, but we cannot rule out the variations smaller than 15 seconds. A linear fit without a orbiting planet is consistent with the full data set.

4.2 HS0705+6700

Figure 5 Shows the O-C timing residuals versus epoch computed using linear ephemeris,

$$\text{BJD}_{\min} = 2451822.76201 + 0.09564609 \cdot E \quad (13)$$

along with our 2-component model (solid blue line), 3-component model (solid green line) and the one-component model of Bogensberger et al. 2017 (dashed red line). Tables 4 and 5 list the model parameters of these models. We note that in order to conform to our linear ephemeris, we added 30° to their periastron angle (ω).

It is clear that the previously published one-component model of Bogensberger et al. starts to deviate strongly from the observed timing data starting shortly after the publication of the model. This discouraging trend has been seen for several other eclipsing sdB binary exoplanet detection, as previously noted. Also, we did not plot the recent two component solution proposed by Sale et al. (2020) since we could not determine their ephemeris or interpret orbital parameters of their model from their paper.

An expanded view of the O-C fits for both models is shown in Fig. 6, along with the $\pm 1\sigma$ posterior spread from the EMCEE solutions. Both solutions are stable, as seen in the MEGNO plots (Fig. 7)

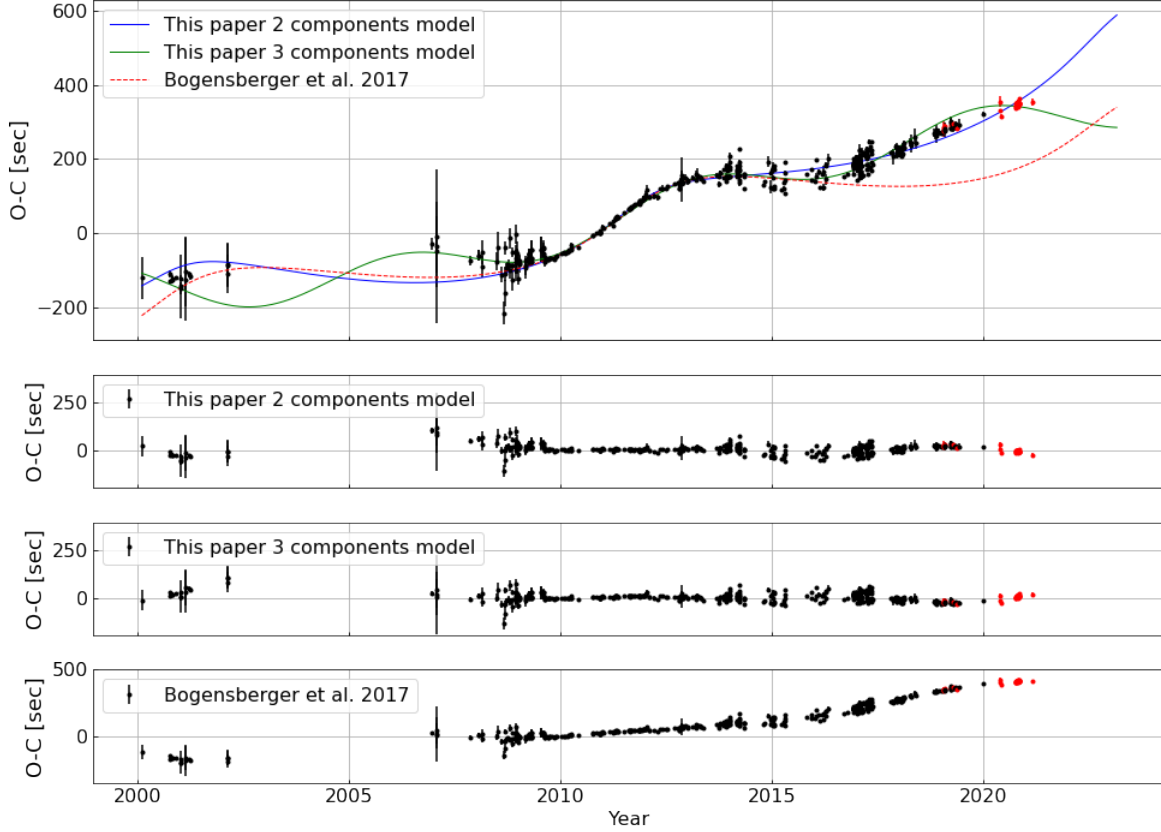


Figure 5. *Upper panel:* HS0705+6700 O-C plot with two component (blue line) and three component (green line) models overlaid. Also shown (red line) is the one component model of [Bogensberger et al. 2017](#). The black data points are from the literature, while the red data points are from Table 2. *Lower panels:* O-C differences between observed O-C and model predictions.

and the numerical orbit integration plots of eccentricity and semi-major axis over 10 Myr (Fig. 8). Finally, Fig. 9 shows the two-dimensional projections of the sample covariances for both models. They demonstrate that both models have well-defined parameters with small fractional uncertainties. However, they are degenerate, since both models provide very similar fits. Since both the least-squares and EMCEE solutions depend on the initial guesses, it is possible that a large number of solutions exist with similar fits.

4.3 HW Virginis

Figure 10 Shows the O-C timing residuals versus epoch using the linear ephemeris

$$\text{BJD}_{\min} = 2450280.28596 + 0.116719519 \cdot E \quad (14)$$

On the right of each panel are plots of eccentricity and semi-major axes of all model components vs. epoch as computed by numerical integration using REBOUND with time steps of 0.1 yr. The plots also show two model fits:

- The upper panel shows a three component model (Table 6)

computed using the minimization scheme described in section 3, with a Bayesian prior $\beta > 1.05$ for all component pairs, where β is the normalized Hill constraint. This solution is stable for at least 10 Myr, but is a very poor fit to the timing data ($\chi^2 \approx 70$).

- The lower panel shows a 4-component model (Table 7), also computed using the minimization scheme in section 3, but without the Hill stability prior. This provides a much better fit ($\chi^2 \approx 7$) but is highly unstable over short time intervals (several hundred years).

This unfortunate scenario (acceptable O-C model fits are invariably unstable) was also found by ([Brown-Sevilla et al. 2021](#)) who analyzed a series of best-fit six multi-component models for HW Vir. In the section we discuss possible alternatives to pure substellar component models.

5 ALTERNATIVE EXPLANATIONS FOR ECLIPSE TIMING VARIATIONS

As mentioned previously, eclipse timing variations can be caused by mechanisms other than gravitational perturbation by orbiting cir-

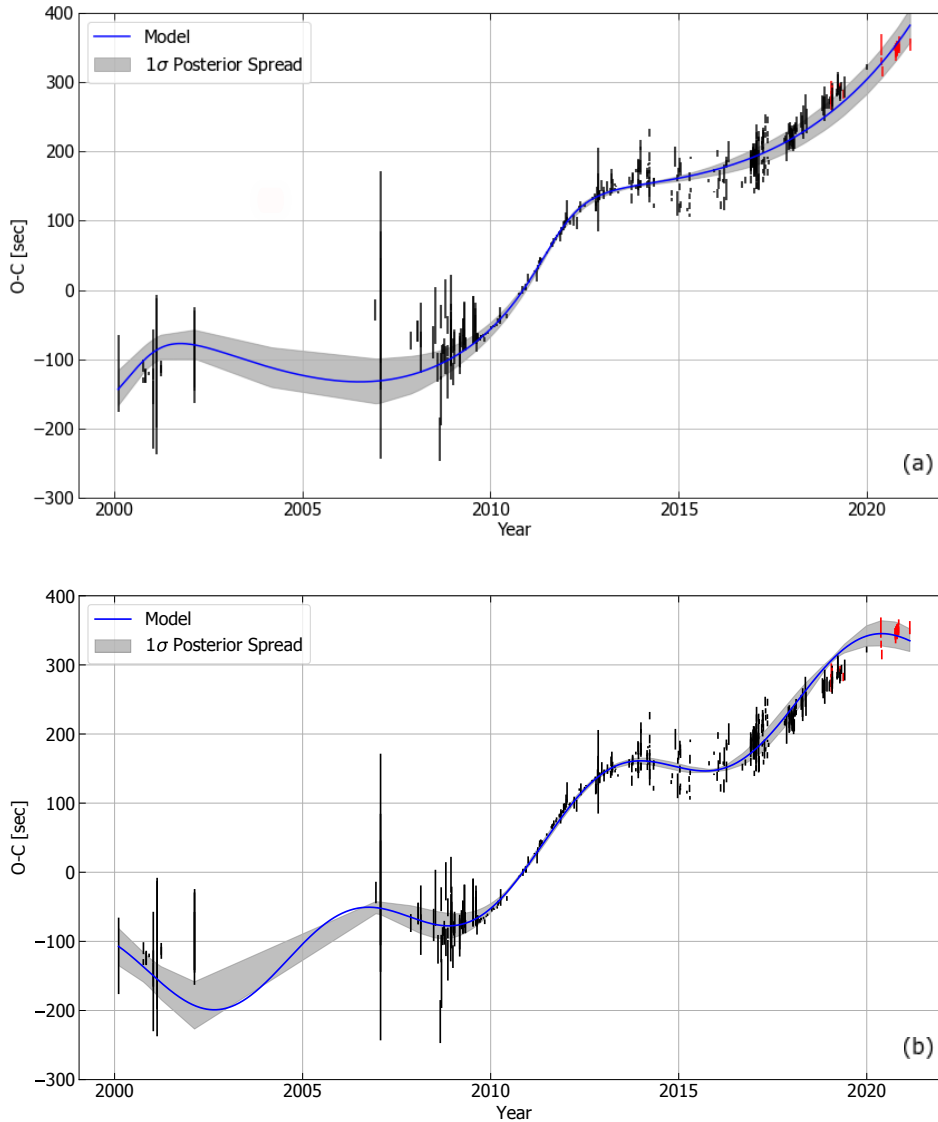


Figure 6. HS0705+6700 O-C plot with overlaid (a) two component model (Table 4, upper panel), and (b) three component model (Table 5, lower panel). The gray shaded area is the $\pm 1\sigma$ spread of the EMCEE posterior samples distribution.

cumbinary masses. These include interbinary mass transfer, apsidal motion, and changes in the moment of inertia caused by magnetic activity on one of the components (Applegate mechanism).

For sdB binaries, mass transfer is ruled out since they are detached systems. Apsidal precession can result from (general relativistic) gravitational radiation and by tidal effects caused by an asymmetric mass distribution in one (or both) components. Lee et al. (2009) has shown that gravitational radiation for the sdB binary HW Vir, and by extension other similar systems including HS0705+6700, would result in time variations at about 2 dex smaller than observed.

Ruling out apsidal effects is more problematic since they depend on the tidal distortion of the internal mass distribution (via the internal structure constant k_2 , Sirotkin & Kim 2009) which is not well-characterized for these systems. Almeida et al. (2020) recently considered tidal and rotation apsidal effects on eclipse timing variations for the PCEB GK Vir. They found that apsidal is less likely than substellar component model, but could not rule it out as a contributing

factor. In addition, apsidal effects will produce strictly periodic signatures in O-C plots, which is not observed for the binaries considered in this paper. Hence, we do not consider apsidal effects further, but examine the possible contribution of Applegate-type mechanisms.

Applegate (Applegate & Patterson 1987; Applegate 1992) proposed that orbital period changes in close binaries may result from a variable quadrupole moment produced by magnetic activity in the outer convection zone of one of the stars. For sdB binaries, this is likely to be the low-mass secondary, which is fully convective. Although we are not aware of any direct evidence for magnetic fields in any sdB secondary star, there is ample evidence for strong (kiloGauss) surface fields in many late-type (M0-M5) main sequence single stars similar to the secondaries in sdB binaries (e.g., Kochukhov 2020, and references therein). Also, tidal locking will ensure that the rotation of the secondary is very rapid, enhancing the prospects for a robust magnetic dynamo.

The original Applegate mechanism assumed a time-dependent

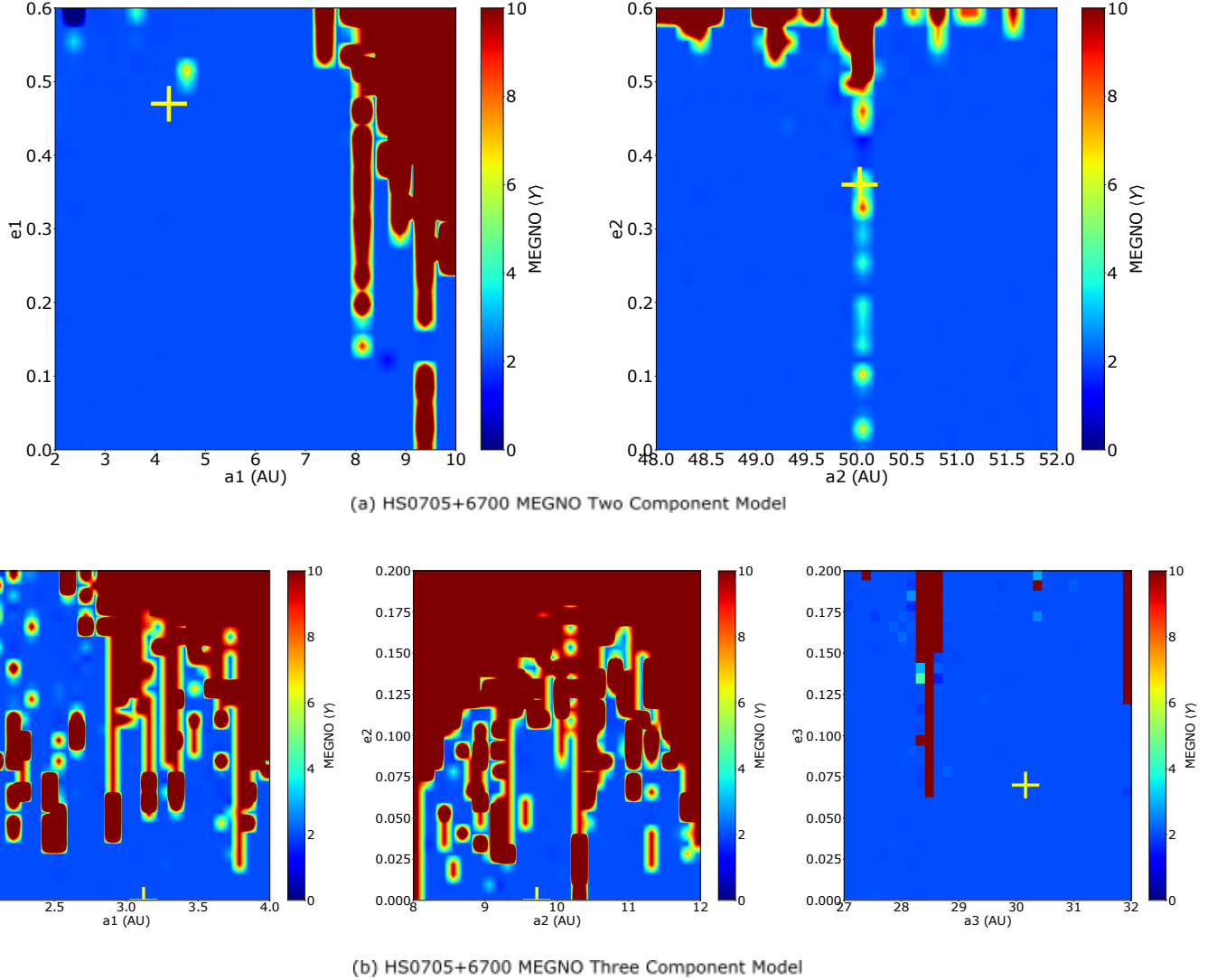


Figure 7. HS0705+6700 MEGNO plots of eccentricity vs. semi-major axis for (a) two component model (b) three component model. The best-fit parameters for each component (Tables 4, 5) are shown as yellow crosses. MEGNO values less than 2 are consistent with non-chaotic behavior (e.g., Hinse et al. 2010).

gravitational quadrupole moment modulated by the magnetic activity cycle in an outer thin shell of the active star. An increasing quadrupole moment results in a stronger gravitational field, driving a decreasing orbital radius and a consequent reduction of the binary period, and conversely. However, it was subsequently found that energy required to drive quadrupole moment variations of the secondary star that could account for the ETV’s was inconsistent with observed luminosity changes in many close binaries (Völschow, M. et al. 2016).

Several recent papers have analyzed modifications to the original Applegate model using more complex 2-shell models, generalizing the magnetohydrodynamic effects of internal magnetic fields, and considering different types of dynamo models (e.g., Lanza et al. 1998; Lanza 2006; Navarrete, F. H. et al. 2018; Völschow, M. et al. 2018; Navarrete et al. 2019). Here we consider the recent model of Lanza (2020) which is based on angular momentum exchange between the spin of the active component and the orbital motion.

Spin–orbit coupling is produced by a non-axisymmetric component of the gravitational quadrupole moment of the active star caused by an assumed persistent non-axisymmetric internal magnetic field.

5.0.1 Hybrid models with substellar components and Applegate-type modulation

As we have seen, the best-fit stable orbit model fits for both HS0705 and HW Vir are not fully in agreement with the observed O-C data, with residual differences of order 10 sec and 60 sec over 10-20 year timescales for HS0705 and HW Vir respectively (Figs. 5, 10). We now consider the question of whether the ETV variations may result from a combination of substellar component perturbation and Applegate-Lanza effects.

The change in fractional angular velocity Ω of the secondary is related to the observed fractional period changes by (Lanza 2020,

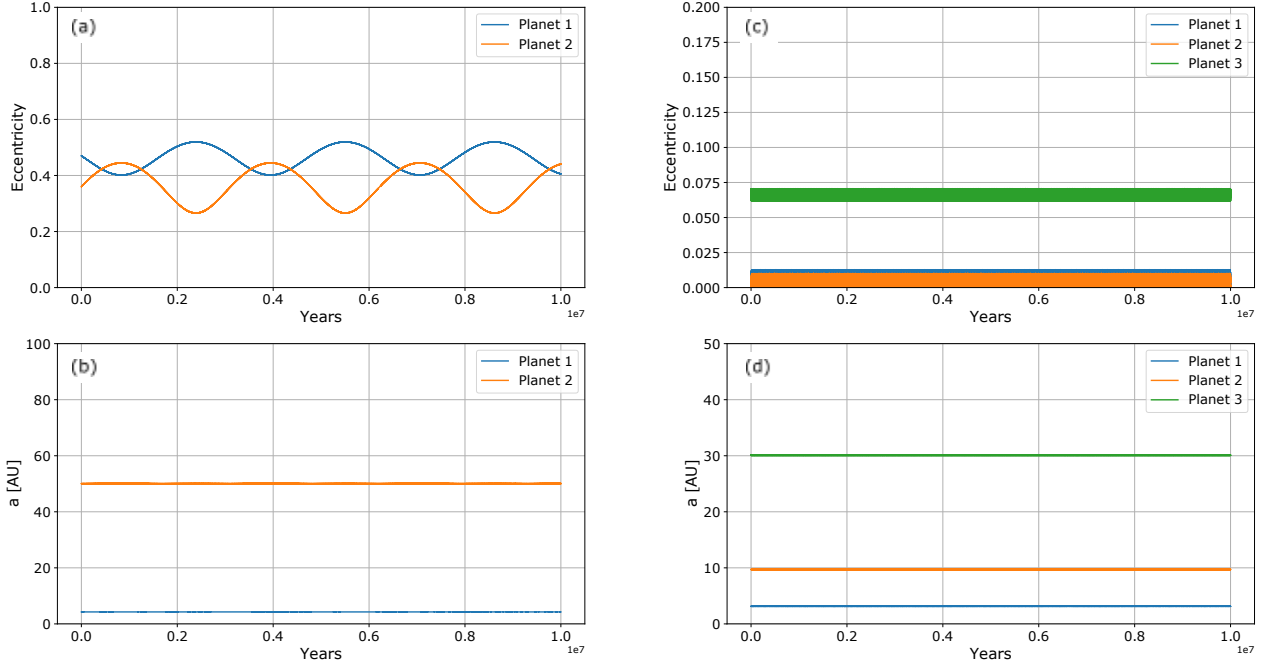


Figure 8. HS0705+6700 stability plot for 2 and 3 component models listed in Table 4 and 5: (a) 2-component time evolution of eccentricity over 10 Myr, (b) Semi-major axis for both components over 10 Myr. (c,d) Same as (a,b), but for 3-component model, listed in Table 5.

Table 4. HS0705+6700 Two Component Model

Parameter	Fitted Values	Unit	
Inner Binary			
T_0	2451822.76201	BJD	
P_0	0.095646609	day	
\dot{P}	$19.9^{+0.3}_{-0.2}$	10^{-12} s/s	
Substellar Components			
	LTT 1	LTT 2	
P	$11.05^{+0.04}_{-0.19}$	449^{+56}_{-179}	yr
e	$0.47^{+0.01}_{-0.04}$	$0.36^{+0.08}_{-0.13}$	
K	$69.3^{+0.17}_{-0.8}$	206.9^{+18}_{-56}	sec
$asin(i)$	$4.27^{+0.01}_{-0.05}$	50.3^{+4}_{-13}	AU
ω	$0.67^{+0.03}_{-0.04}$	$5.6^{+0.05}_{-0.20}$	radian
Min. Mass	$21.96^{+0.19}_{-0.09}$	$5.6^{+0.4}_{-0.5}$	M_{Jup}

eqn. 56)

$$\frac{\Delta\Omega}{\Omega} = -\frac{ma^2}{3I_s} \frac{\Delta P}{P} \quad (15)$$

Where m in the reduced mass of the binary, a is the semi-major axis of the binary, I_s is the moment of inertia about the active (secondary) star spin axis, and $\Delta P/P = \Delta t/T$ is the fractional change in the period, or equivalently the O-C deviations t over the timescale T of the O-C data. The consequent change in rotational energy is

$$\Delta E_{rot} = I_s \Omega \Delta\Omega \quad (16)$$

Combining these equations, the dependence on I_p cancels, giving,

$$\Delta E_{rot} = -\left[mr_0^2\Omega^2\right] \frac{\Delta t}{3T} \quad (17)$$

For both HS0705+6700 and HW Vir, the average timing residuals of the substellar companion model fits to the observed O-C data are both of order 10 sec over 10 yr ($\Delta t/3T \sim 10^{-8}$), while the bracketed term evaluates to $3 \cdot 10^{40}$ J, so the change in rotational energy is

$$\Delta E_{rot} \approx -3 \cdot 10^{32} \text{ J} \quad (18)$$

We can compare this with the maximum energy available from luminosity changes over the timescale for O-C variability in the secondary star. From Table 3,

$$E_{max} = L \cdot t \sim 0.002 L_{sun} \cdot 10 \text{ yr} \sim 3 \cdot 10^{32} \text{ J} \quad (19)$$

Remarkably, this is the same as the energy loss required to account for residual changes in the O-C model fits, but would be only $\sim 10\%$ of the entire O-C deviations from a constant period were due to

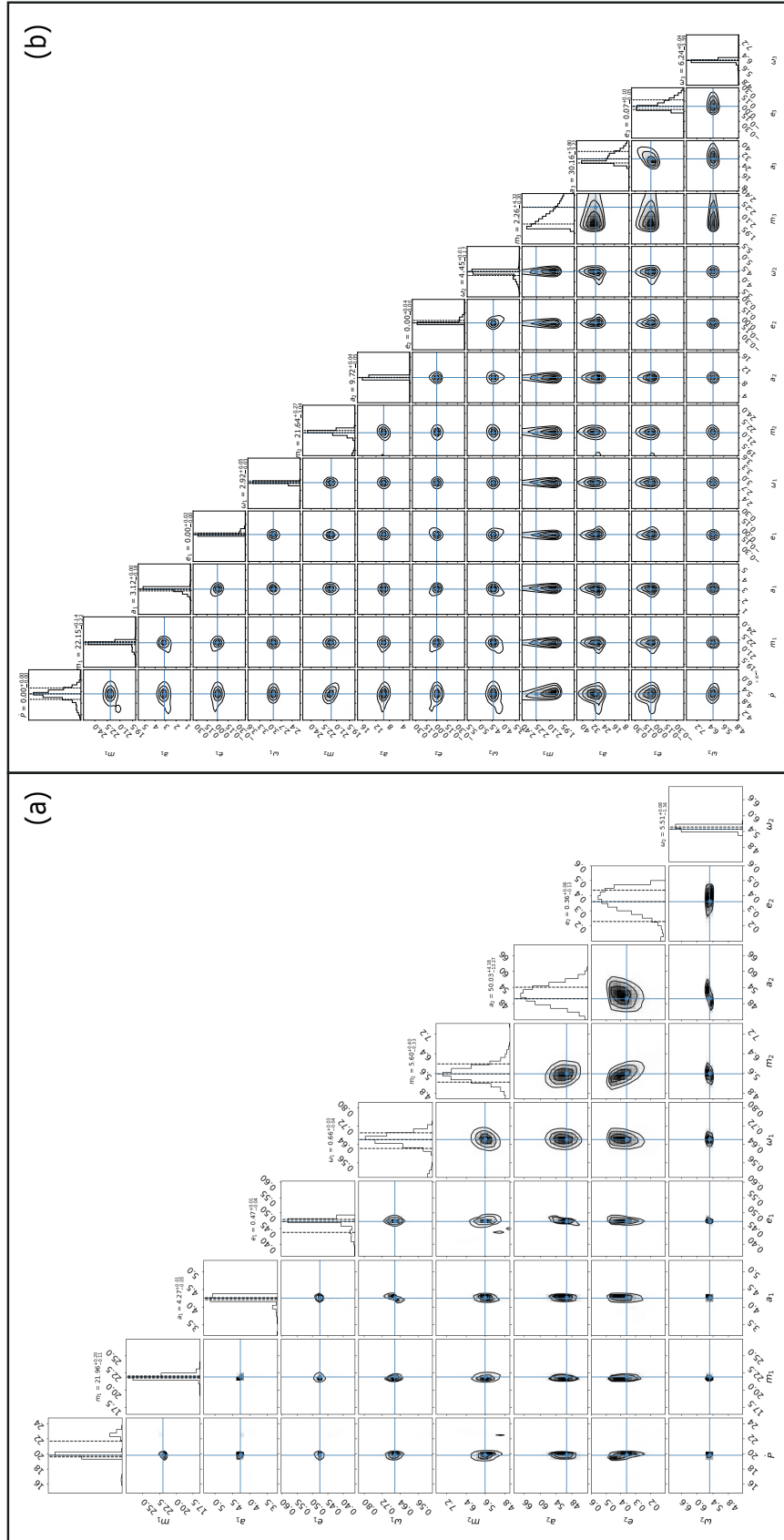


Figure 9. Joint posterior model parameter probability distributions for (a) 2-component, and (b) 3-component models for HS0705+6700, as listed in Tables 4, 5 respectively. The blue lines are median values, and contours 16%, 50%, and 84% quantiles.

Table 5. HS0705+6700 Three Component Model

Parameter	Fitted Values			Unit
Inner Binary				
T_0	2451822.76201			BJD
P_0	0.095646609			day
\dot{P}	$5.24^{+0.24}_{-0.26}$			10^{-12} s/s
Substellar Components				
	LTT 1	LTT 2	LTT3	
P	$6.9^{+0.0}_{-0.6}$	$38^{+0.15}_{-0.30}$	$211^{+60.8}_{-33.8}$	yr
e	$0.0^{+0.02}_{-0.0}$	$0.0^{+0.04}_{-0.0}$	$0.07^{+0.1}_{-0.05}$	
K	$49.7^{+0.0}_{-2.87}$	$151^{+0.65}_{-3.76}$	$49^{+188.5}_{-5.6}$	sec
$asin(i)$	$3.12^{+0.0}_{-0.18}$	$9.72^{+0.04}_{-0.05}$	$30.2^{+5.8}_{-3.22}$	AU
ω	$2.92^{+0.05}_{-0.03}$	$4.45^{+0.01}_{-0.17}$	$6.24^{+0.04}_{-3.6}$	radian
Min. Mass	$22.15^{+0.14}_{-0.22}$	$21.64^{+0.27}_{-3.04}$	$2.26^{+4.3}_{-0.2}$	M_{Jup}

Table 6. HW Vir Three Component Stable Model

Parameter	Fitted Values			Unit
Inner Binary				
T_0	2450280.28596			BJD
P_0	0.116719519			day
\dot{P}	$-12.4 \pm (0.34)$			10^{-12} s/s
Substellar Components				
	LTT 1	LTT 2	LTT3	
P	7.8 ± 0.14	30.7 ± 0.33	159.2 ± 13.84	yr
e	0.03 ± 0.02	0.03 ± 0.02	0.13 ± 0.04	
K	7 ± 0.2	98.4 ± 0.76	100.5 ± 6.31	sec
$asin(i)$	3.37 ± 0.04	8.46 ± 0.06	25.19 ± 1.46	AU
ω	0.03 ± 0.22	2.77 ± 0.02	5.74 ± 0.05	radian
Min. Mass	2.85 ± 0.37	15.91 ± 0.41	5.46 ± 0.38	M_{Jup}

Table 7. HW Vir Four Component Unstable Model

Parameter	Fitted Values				Unit
Inner Binary					
T_0	2450280.28596				BJD
P_0	0.116719519				day
\dot{P}	$-12.6 \pm (0.23)$				10^{-12} s/s
Substellar Components					
	LTT 1	LTT 2	LTT3	LTT4	
P	7.32 ± 0.03	11.94 ± 0.08	31.36 ± 0.82	437.03 ± 29.97	yr
e	0.04 ± 0.03	0.0 ± 0.0	0.5 ± 0.02	0.3 ± 0.13	
K	8.7 ± 0.04	18.8 ± 0.09	122.1 ± 2.15	267.1 ± 15.53	sec
$asin(i)$	3.23 ± 0.01	4.48 ± 0.02	8.59 ± 0.15	49.44 ± 2.26	AU
ω	0.02 ± 0.06	3.6 ± 0.05	2.9 ± 0.01	6.08 ± 0.02	deg
Min. Mass	3.76 ± 0.12	5.84 ± 0.1	19.8 ± 0.27	7.53 ± 0.84	M_{Jup}

an Applegate-Lanza mechanism. This suggests that the observed O-C variations could be explained by a combination of substellar companions accounting for the bulk of the ETV's, with a Lanza-Applegate mechanism contributing about 10% of the total.

5.0.2 Tidal Synchronization Timescale

Another relevant dynamical timescale is the tidal synchronization time i.e., the timescale in which tides on the secondary dissipate the kinetic energy of asynchronous rotation (Lanza 2020),

$$t_{sync} = \frac{2Q}{9} \frac{M_T}{m_p^2} \frac{I_s}{\sqrt{GM_T R}} \left(\frac{a}{R}\right)^{9/2} \quad (20)$$

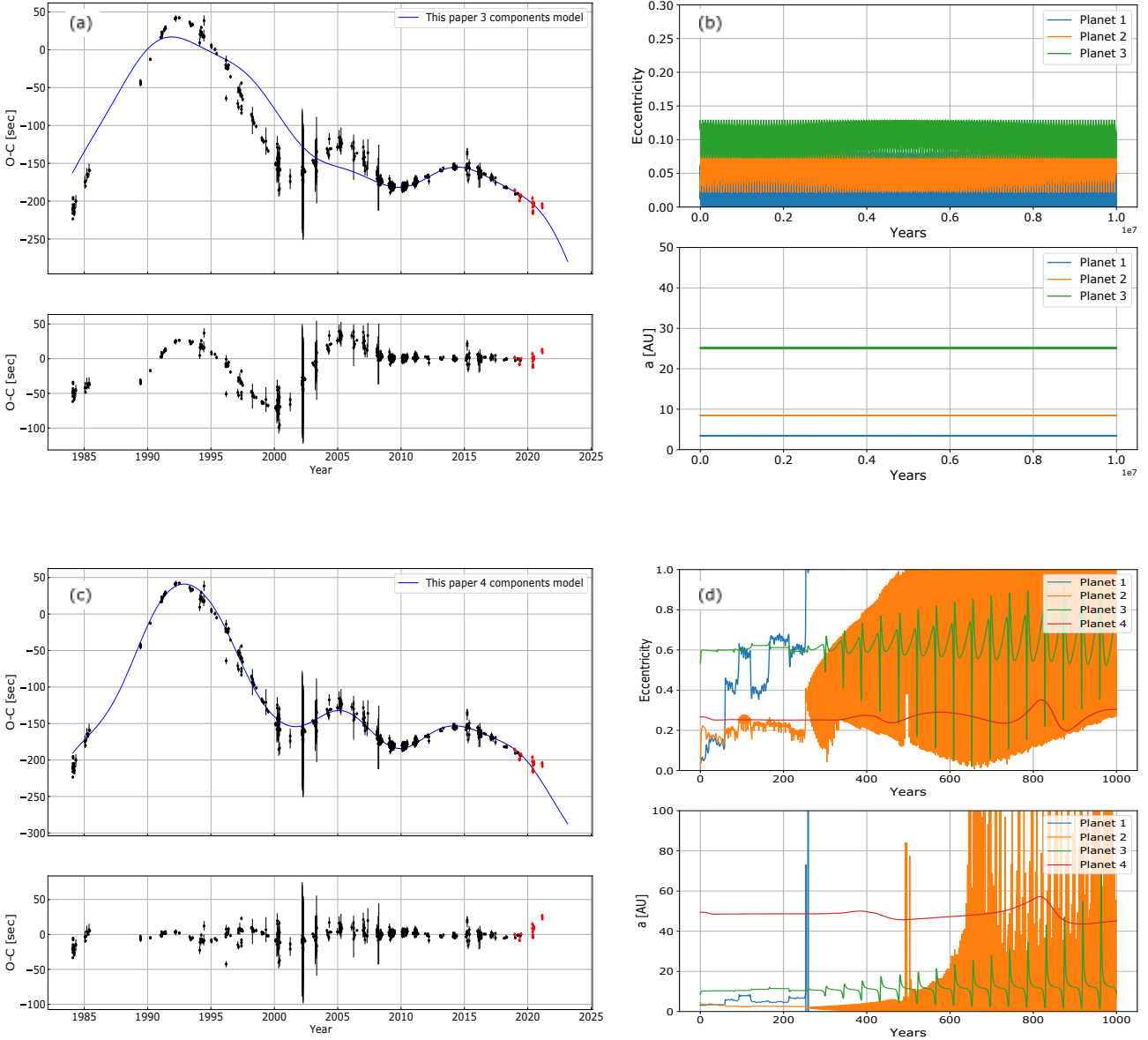


Figure 10. HW Vir O-C times of primary minima computed using the linear ephemeris given in Equation 14. Black points are archival times of minima from the literature, red points are new times of minima from Table 2, and blue lines are model predictions. (a) Best-fit 3-component model (Table 6) subject to the constraint that the model is stable i.e., all pairwise component normalized Hill parameters exceed 1.05. (b) Eccentricity and semi-major axes of all three components over 10 Myr. This solution is stable but is a very poor fit ($\chi_r^2 \approx 70$) to the timing data. (c) Best-fit 4-component model (Table 7). (d) Eccentricity and semi-major axes of all four components over 1000 yr. The four component model provides a much improved fit ($\chi_r^2 \approx 7$) but is highly unstable. We conjecture that the observed ETV’s may be result from a combination of gravitational perturbations by substellar companions and a Applegate-Lanza mechanism.

where Q is a dimensionless tidal quality factor that characterizes the efficiency of tidal energy dissipation in the active (secondary) component, M_T is the total mass of the binary system, m_p is the primary mass, a is the binary semi-major axis, and R is the active star radius. Following Lanza (2020), we assume $Q \sim 10^5 - 10^6$ corresponding to strong tidal coupling due to nearly synchronous rotation. For the moment of inertia I_s , we use the numerical expression of Criss

& Hofmeister (2015) for a fully convective secondary star with a polytropic index $n = 1.5$,

$$I_s = 0.2 m_{sec} R_{sec}^2 \quad (21)$$

Using stellar parameters list in Table 3, we find tidal synchronization timescales $t_s = 4 - 40$ yr and $10 - 100$ yr for HS0705 and HW Vir respectively. These times are comparable to the observed O-C variations, so tidal synchronization may dictate the timescale for spin-orbit coupling rather than magnetic activity timescales.

6 SUMMARY AND CONCLUSIONS

In this paper, we have reported new eclipse timing observations of three post-common envelope binary systems. We combined these observations with previously published timing data to investigate whether the eclipse timing variations from a linear ephemeris could be explained by the gravitational influence of orbiting substellar companions. We used models comprising multiple substellar companions in coplanar orbits parallel to the observer’s line of sight, adjusting their orbital parameters and masses to best fit the observed timing variations.

For one of the three binaries (HS2231+2441), nearly all times of minima are consistent with a linear ephemeris. Hence, there is no evidence for substellar companions in this system, although they cannot be ruled out if the masses are small. However for the remaining two binaries, there are large timing variations (ETV) from the linear trend, indicating the presence of one or more gravitationally perturbing effects. We focused on finding orbital parameters and masses of companions that could account for the observed ETV’s by varying the masses and orbital elements to best-fit the observed ETV time signature using a least-squares minimization.

In order to ensure that the substellar components had stable orbits, the minimization function included a Hill stability ‘penalty’ ansatz that increases sharply when the minimum separation between adjacent components was smaller than one Hill radius. We also used a Bayesian inference algorithm to better characterize the uncertainties of the derived orbital parameters and masses. In addition, we used the Hill stability criterion $H > 1$ as a prior to restrict orbital solutions only to those that were plausibly long-term stable i.e., at least as long as the assumed time scale for common-envelope evolution (Schreiber & Gänsicke 2003; Ivanova et al. 2013).

Finally, we checked stability timescales for each model using a numerical N-body symplectic time-step integrator (WHFAST) and an algorithm to detect the onset of chaotic behavior (MEGNO). We ran both the numerical integrations and chaos indicator time evolutions for 10^7 years.

For HS0705+6700, we found 2 and 3-component models that reproduced the observed ETV time history reasonably well and that were stable on long time scales ($\approx 10^8$ yr). However, the fits were not statistically convincing, with reduced chi-squares of the fitted models in the range 10–15, although this may be partly a result of underestimated uncertainties in previously published timing measurements (cf. Hinse et al. 2014). In addition, the model solutions were degenerate: Both the 2 and 3 component models fit the timing data equally well, but the solutions are very different. Different initial starting values would likely have resulted in other stable, but very different solutions.

For HW Vir, we found no stable solutions that could fit the ETV time signature, although it was possible to find adequate 3 and 4 component fits, albeit with highly unstable orbits. This has also been the unfortunate conclusion of several previous studies of HW Vir (e.g., Horner et al. 2012; Brown-Sevilla et al. 2021) and although not definitive, this strongly suggests that substellar companions cannot account for all of the ETV time history observed in these (and likely other) PCEB binaries.

Therefore, we investigated whether some fraction of the observed variations could be caused by an Applegate mechanism in which the secondary star’s gravitational quadrupole moment is altered by magnetic activity. Although the original Applegate mechanism was found to be energetically insufficient to account for the observed timing variations in sdB binaries (e.g., Völschow, M. et al. 2016),

various revisions of the mechanism have been suggested that may account for at least a fraction of the observed variations.

We applied the model of Lanza (2020), in which spin–orbit coupling is produced by an active (secondary) star’s non-axisymmetric internal magnetic field creates a non-axisymmetric gravitational quadrupole moment. Using this model, we find that the predicted timing variations could account for perhaps 10% of the observed O-C variability, although this result is uncertain, since it is dependent on poorly constrained binary system parameters such as the tidal energy dissipation and the internal mass distribution of the stars. Hence, we posit that the observed O-C variations could result from a hybrid model in which substellar companions account for a largest fraction of the timing variations, but that a Lanza-type mechanism contributes the remainder.

ACKNOWLEDGEMENTS

This research made use of the LMFIT nonlinear least-square minimization Python library, and Astropy, a community developed core Python package for Astronomy. We also made use of emcee, an MIT licensed pure-Python implementation of the affine invariant Markov chain Monte Carlo (MCMC) ensemble sampler (Goodman & Weare 2010). We also used the excellent Python module `corner.py` to visualize multidimensional results of Markov Chain Monte Carlo simulations (Foreman-Mackey 2016). Numerical orbit integrations in this paper made use of the REBOUND N-body code (Rein & Liu 2012). The simulations were integrated using WHFAST, a Wisdom-Holman symplectic integrator (Rein & Tamayo 2015).

We are grateful to David Pulley, John Mallett and the Altair Group for their contribution of times of minima for HS0705+6700 on Dec 29th, 2019, and times of minima for HW Vir on June 6th, 2019. We are also grateful to Prof. Antonino Lanza for several very insightful communications. The Iowa Robotic Observatory is funded by the College of Liberal Arts at the University of Iowa.

DATA AVAILABILITY

We have provided Table 2 as our new mid-eclipse timing data of three post-common envelope binaries. The light curves available on request from the corresponding author.

REFERENCES

- Almeida L. A., Daminieli A., Rodrigues C. V., Pereira M. G., Jablonski F., 2017, *MNRAS*, 472, 3093
- Almeida L. A., Pereira E. S., Borges G. M., Daminieli A., Michtchenko T. A., Viswanathan G. M., 2020, *Monthly Notices of the Royal Astronomical Society*, 497, 4022
- Applegate J. H., 1992, *ApJ*, 385, 621
- Applegate J. H., Patterson J., 1987, *ApJ*, 322, L99
- Baran A. S., et al., 2018, *MNRAS*, 481, 2721
- Bear E., Soker N., 2014, *Monthly Notices of the Royal Astronomical Society*, 444, 1698
- Beuermann K., et al., 2012a, *A&A*, 540, A8
- Beuermann K., Dreizler S., Hessman F. V., Deller J., 2012b, *A&A*, 543, A138
- Bogensberger D., Clarke F., Lynas-Gray A. E., 2017, *Open Astronomy*, 26, 134
- Brown-Sevilla S. B., et al., 2021, *Monthly Notices of the Royal Astronomical Society*, 506, 2122
- Carter J. A., Yee J. C., Eastman J., Gaudi B. S., Winn J. N., 2008, *The Astrophysical Journal*, 689, 499

- Chambers J., Wetherill G., Boss A., 1996, *Icarus*, 119, 261
- Cincotta P. M., Simó C., 2000, *Astron. Astrophys. Suppl. Ser.*, 147, 205
- Criss R. E., Hofmeister A. M., 2015, *New Astron.*, 36, 26
- Deeg H. J., 2021, *Galaxies*, 9
- Deeg, H. J. 2015, *A&A*, 578, A17
- Drechsel H., et al., 2001, *A&A*, 379, 893
- Esmer E. M., Baştürk Ö., Hinse T. C., Selam S. O., Correia A. C. M., 2021, *A&A*, 648, A85
- Foreman-Mackey D., 2016, *Journal of Open Source Software*, 1, 24
- Foreman-Mackey D., Hogg D. W., Lang D., Goodman J., 2013, *PASP*, 125, 306
- Gladman B., 1993, *Icarus*, 106, 247
- Goodman J., Weare J., 2010, *Communications in Applied Mathematics and Computational Science*, 5, 65
- Han Z., Podsiadlowski P., Maxted P. F. L., Marsh T. R., Ivanova N., 2002, *MNRAS*, 336, 449
- Han Z., Podsiadlowski P., Maxted P. F. L., Marsh T. R., 2003, *Monthly Notices of the Royal Astronomical Society*, 341, 669
- Hasegawa M., Nakazawa K., 1990, *A&A*, 227, 619
- Heber U., 2009, *Annual Review of Astronomy and Astrophysics*, 47, 211
- Heber U., 2016, *Publications of the Astronomical Society of the Pacific*, 128, 082001
- Hinse T. C., Christou A. A., Alvarrellos J. L. A., Goździewski K., 2010, *MNRAS*, 404, 837
- Hinse T. C., Horner J., Lee J. W., Wittenmyer R. A., Lee C.-U., Park J.-H., Marshall J. P., 2014, *A&A*, 565, A104
- Horner J., Hinse T. C., Wittenmyer R. A., Marshall J. P., Tinney C. G., 2012, *MNRAS*, 427, 2812
- Horner J., Wittenmyer R., Hinse T., Marshall J., Mustill A., 2014, *Wobbling Ancient Binaries - Here Be Planets?* ([arXiv:1401.6742](https://arxiv.org/abs/1401.6742))
- İbanoğlu C., Çakırlı Ö., Taş G., Evren S., 2004, *A&A*, 414, 1043
- Icko J. I., Livio M., 1993, *Publications of the Astronomical Society of the Pacific*, 105, 1373
- Irwin J. B., 1952, *ApJ*, 116, 211
- Irwin J. B., 1959, *AJ*, 64, 149
- Ivanova N., et al., 2013, *A&ARv*, 21, 59
- Kilkenny D., Marang F., Menzies J. W., 1994, *MNRAS*, 267, 535
- Kilkenny D., Keuris S., Marang F., Roberts G., van Wyk F., Ogloza W., 2000, *The Observatory*, 120, 48
- Kilkenny D., van Wyk F., Marang F., 2003, *The Observatory*, 123, 31
- Kiss L. L., Csák B., Szatmáry K., Fűrész G., Sziládi K., 2000, *A&A*, 364, 199
- Kochukhov O., 2020, *The Astronomy and Astrophysics Review*, 29, 1
- Kwee K. K., van Woerden H., 1956, *Bull. Astron. Inst. Netherlands*, 12, 327
- Lanza A. F., 2006, *MNRAS*, 369, 1773
- Lanza A. F., 2020, *MNRAS*, 491, 1820
- Lanza A. F., Rodono M., Rosner R., 1998, *MNRAS*, 296, 893
- Lee J. W., Kim S.-L., Kim C.-H., Koch R. H., Lee C.-U., Kim H.-I., Park J.-H., 2009, *The Astronomical Journal*, 137, 3181
- Lohr M. E., et al., 2014, *A&A*, 566, A128
- Marsh T. R., 2018, *Circumbinary Planets Around Evolved Stars*. Springer International Publishing, Cham, pp 2731–2747, doi:10.1007/978-3-319-55333-7_96, https://doi.org/10.1007/978-3-319-55333-7_96
- Martin D. V., 2018, *Populations of Planets in Multiple Star Systems*. Springer International Publishing, Cham, pp 2035–2060, doi:10.1007/978-3-319-55333-7_156, https://doi.org/10.1007/978-3-319-55333-7_156
- Mayor M., Queloz D., 1995, *Nature*, 378, 355
- Nasiroglu I., et al., 2017, *AJ*, 153, 137
- Navarrete, F. H. Schleicher, D. R. G. Zamponi Fuentealba, J. Völschow, M. 2018, *A&A*, 615, A81
- Navarrete F. H., Schleicher D. R. G., Kárpáthy P. J., Schober J., Völschow M., Mennickent R. E., 2019, *Monthly Notices of the Royal Astronomical Society*, 491, 1043
- Nebot Gómez-Morán A., Gänsicke B. T., Schreiber M. R., Schwöpe A. D., 2011, in Schmidtbreick L., Schreiber M. R., Tappert C., eds, *Astronomical Society of the Pacific Conference Series Vol. 447, Evolution of Compact Binaries*. p. 187
- Østensen R., Oreiro R., Drechsel H., Heber U., Baran A., Pigulski A., 2007, in Napiwotzki R., Burleigh M. R., eds, *Astronomical Society of the Pacific Conference Series Vol. 372, 15th European Workshop on White Dwarfs*. p. 483
- Parsons S. G., et al., 2013, *Monthly Notices of the Royal Astronomical Society: Letters*, 438, L91
- Pulley D., Faillace G., Smith D., Watkins A., Owen C., 2015, *Journal of the British Astronomical Association*, 125, 284
- Pulley D., Faillace G., Smith D., Watkins A., von Harrach S., 2018, *A&A*, 611, A48
- Qian S.-B., Dai Z., Zhu L.-Y., Liu L., He J.-J., Liao W.-P., Li a., 2008, *The Astrophysical Journal Letters*, 689, L49
- Qian S.-B., et al., 2009, *The Astrophysical Journal*, 695, L163
- Qian S. B., et al., 2010, *Ap&SS*, 329, 113
- Qian S. B., et al., 2013, *MNRAS*, 436, 1408
- Rein H., Liu S. F., 2012, *A&A*, 537, A128
- Rein H., Spiegel D. S., 2015, *MNRAS*, 446, 1424
- Rein H., Tamayo D., 2015, *MNRAS*, 452, 376
- Sale O., Bogensberger D., Clarke F., Lynas-Gray A. E., 2020, *Monthly Notices of the Royal Astronomical Society*, 499, 3071
- Schleicher D. R. G., Dreizler S., 2014, *A&A*, 563, A61
- Schleicher D. R. G., Dreizler S., Völschow M., Banerjee R., Hessman F. V., 2015, *Astronomische Nachrichten*, 336, 458
- Schreiber M. R., Gänsicke B. T., 2003, *A&A*, 406, 305
- Schwarz R., Funk B., Zechner R., Bazsó Á., 2016, *Monthly Notices of the Royal Astronomical Society*, 460, 3598
- Shakura N. I., 1985, *Soviet Astronomy Letters*, 11, 224
- Sirotkin F. V., Kim W.-T., 2009, *The Astrophysical Journal*, 698, 715
- Skelton P. L., 2012, *African Skies*, 16, 132
- Smullen R. A., Kratter K. M., Shannon A., 2016, *MNRAS*, 461, 1288
- Tokovinin A., 2014, *The Astronomical Journal*, 147, 87
- Völschow, M. Schleicher, D. R. G. Perdelwitz, V. Banerjee, R. 2016, *A&A*, 587, A34
- Völschow, M. Schleicher, D. R. G. Banerjee, R. Schmitt, J. H. M. M. 2018, *A&A*, 620, A42
- Webbink R. F., 1984, *ApJ*, 277, 355
- Wittenmyer R. A., Horner J., Marshall J. P., Butters O. W., Tinney C. G., 2012, *Monthly Notices of the Royal Astronomical Society*, 419, 3258
- Wittenmyer R. A., Horner J., Marshall J. P., 2013, *Monthly Notices of the Royal Astronomical Society*, 431, 2150
- Wolszczan A., Frail D. A., 1992, *Nature*, 355, 145
- Zorotovic M., Schreiber M. R., 2013, *A&A*, 549, A95
- Zorotovic M., Schreiber, M. R. Gänsicke, B. T. Nebot Gómez-Morán, A. 2010, *A&A*, 520, A86
- Zorotovic M., Schreiber M. R., Gänsicke B. T., 2011, *Astronomy & Astrophysics*, 536, A42
- Çakırlı Ö., Devlen A., 1999, *A&AS*, 136, 27

APPENDIX A: TIME OF MINIMUM UNCERTAINTY ESTIMATES

In this appendix, we evaluate the uncertainty in the time of minimum determination of an eclipsing binary light curve constructed from a series of images with relatively long exposure times and image download times. These pertain especially to observations using relatively small-aperture telescopes, including those reported in this paper.

A standard technique used by many previous authors (more than 1,100 citation!) is the folded-symmetry algorithm described by [Kwee & van Woerden \(1956\)](#). This technique determines the time of minimum by adjusting a trial midpoint time and minimizing the summed squared magnitude difference between points equally time-displaced on either side of the midpoint. The associated uncertainty is determined by fitting a quadratic function and applying standard propagation of errors to fitted minimum value. The technique relies on equally-space data samples and does not account for interpolation errors when this is not the case. Other more sophisticated methods (e.g., [Carter et al. 2008](#); [Deeg, H. J. 2015](#); [Deeg 2021](#)) have addressed eclipse timing uncertainty, but they generally have been restricted to trapezoidal light curves, as observed in exoplanet transits. This is not applicable to short-period binary systems, whose eclipse light curves are much closer to Gaussian profiles (e.g., [Baran et al. 2018](#)).

We evaluated time of minimum uncertainty using a Monte Carlo approach, simulating observed eclipse light curves with a Gaussian profile whose width, depth, and scatter closely resembles the observed light curve. Fig. A1 shows a light curve of HS0705+6700 observed on with the Iowa Robotic telescope, along with the corresponding simulated light curve. The synthetic light curve was made by sampling a Gaussian function with 0.25 magnitude eclipse depth, and 300 sec half-width. We added Gaussian random noise to each sampled point, with a standard deviation $\sigma = 0.025 \times 2.5^{\Delta m}$ where Δm is the differential magnitude difference to the out-of-eclipse level. The synthetic light curve was sampled every 10 msec. We then binned the simulated date into 40 second bins with 10 second time gap between bins, corresponding the the observed image exposure time and download times for HS0705+6700. The magnitude assigned to each image was the computed mean value of 10 msec samples within each bin. The resulting synthetic light curve was fit with a Gaussian profile to determine the time of minimum. This process was repeated 10,00 times with different times of minima varying from -100 sec to +100 sec relative to the nominal zero-point time of minimum. The difference between the true time of minimum and the fitted time of minimum was recorded.

A histogram of the time difference between the best-fit time of minimum and the true minimum for 1,000 realizations is shown in Fig.A2. The 1σ width is 4 seconds.

This paper has been typeset from a $\text{\TeX}/\text{\LaTeX}$ file prepared by the author.

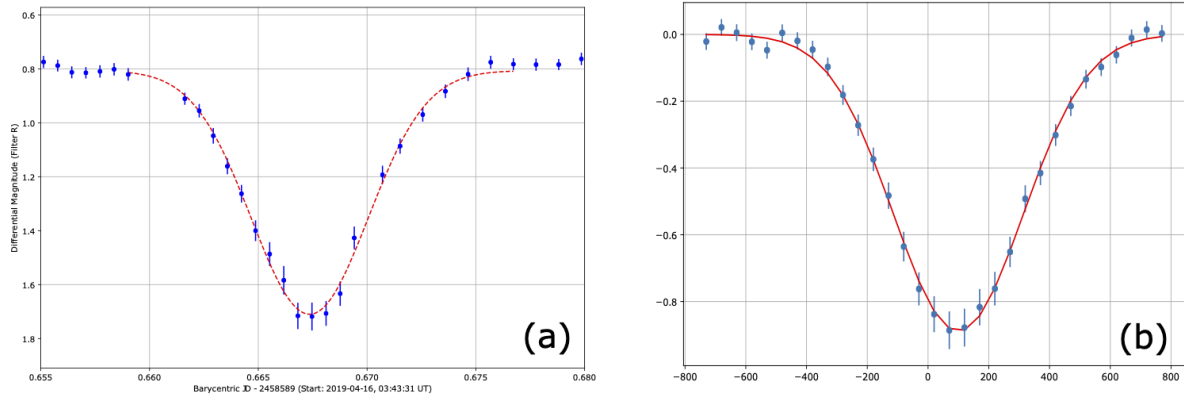


Figure A1. (a) HS0705+6700 primary eclipse 16 April 2019 with LSQ fit Gaussian model.(b) Simulated light curve.

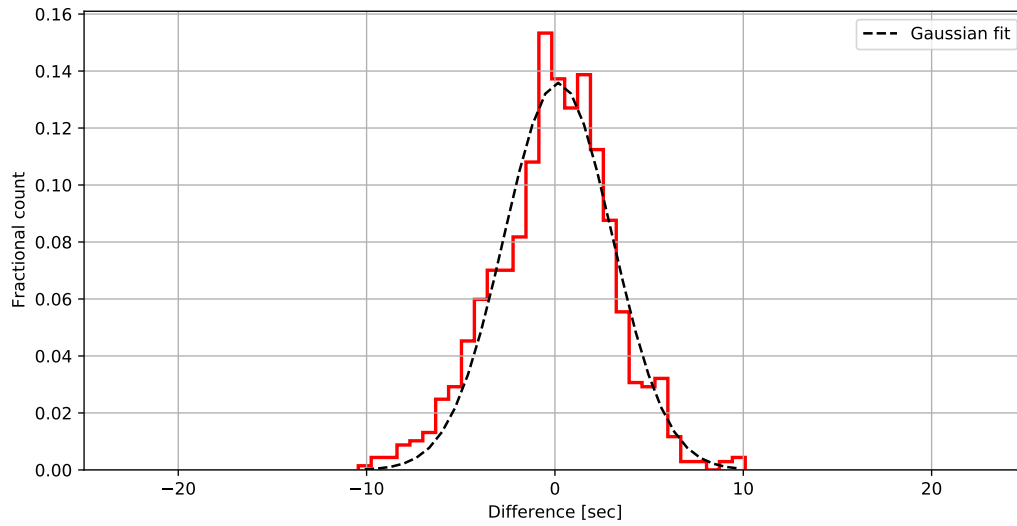


Figure A2. Histogram of time difference between true time of minimum and 10,000 Monte Carlo simulations.